

NINTH EUROPEAN ROTORCRAFT FORUM

Paper No. 18

MODEL HELICOPTER ROTOR BROADBAND NOISE
SOURCES AND SCALING LAWS

Wesley L. Harris
Professor

Department of Aeronautics and Astronautics
Massachusetts Institute of Technology
Cambridge, Massachusetts 02139

and

Niranjan G. Humbad
Senior Engineer
Digital Equipment Corporation
Maynard, Massachusetts 01754

SEPTEMBER 13 - 15, 1983

STRESA, ITALY

MODEL HELICOPTER ROTOR BROADBAND NOISE

SOURCES AND SCALING LAWS

Wesley L. Harris, Professor
Department of Aeronautics and Astronautics
Massachusetts Institute of Technology
Cambridge, Massachusetts 02139

and

Niranjan G. Humbad, Senior Engineer
Digital Equipment Corporation
Maynard, Massachusetts 01754

SUMMARY

This paper summarizes the recent experimental and analytical studies of helicopter rotor broadband noise sources performed at M.I.T. Both low frequency broadband noise (LFBN) and high frequency broadband noise (HFBN) results are presented. The HFBN is due to boundary layer self noise (BLSN). The effects of tip speed, advance ratio, blade loading, free stream turbulence and blade tip geometry on both LFBN and BLSN were studied experimentally. The leading and trailing edge geometries were found to reduce the LFBN by 2-5 dB at low inflow turbulence intensities. A general theoretical model is presented to predict LFBN spectrum and was found in good agreement with the experimental results. Simple scaling laws for both LFBN and BLSN were also found in good agreement with the experimental results. The effects of blade loading on LFBN could not be explained by present theories. In the case of BLSN, saturation of peak sound pressure levels were observed beyond tip Mach number of 0.20.

NOMENCLATURE

B	number of blades	U_f	forward velocity of the rotor
C_T^*	measured thrust coefficient	V	chordwise component of flow velocity relative to the blade
c	blade chord	V_t	tip velocity of the blade ($=\Omega R$)
c_0	speed of sound	\bar{w}	rms velocity of gust turbulence
ΔL	correlation distance	x, y, z	Cartesian coordinate
f	acoustic pressure frequency	β	$\sqrt{1-M^2}$
f_p	peak frequency of BLSN hump	λ	acoustic wavelength
$g(x, k_x, k_y)$	see Eq. (2)	μ	advance ratio
k	wave number of gust	Ω	angular velocity of the rotor blade
k_x, k_y, k_z	components of wave numbers of gust in x, y, and z directions, resp	ω	circular frequency ($= 2\pi f$) of the sound source
L	chordwise integral of surface loading	ω_0	observed circular frequency of sound turbulence spectrum
M, M_t , M_f	Mach numbers corresponding to velocities V, V_t , U_f resp	ϕ_{ww}	angle between the x axis and forward velocity vector of the rotor
P	acoustic pressure	ϕ	density of air
R	blade radius	ρ_0	rotor blade angle with the x axis
r	blade element location from the rotor hub center	ψ	solidarity ratio ($Bc/\pi R$)
r_e	retarded location of source, from the observer	σ	see Eq. (5)
r_l	distance between the observer and the rotor hub center	σ_1	angular location of the observer from the z axis
S_{pp}	power spectral density of acoustic pressure	θ	
T	thrust of rotor		
t	time		

1. Introduction

This paper summarizes the recent experimental and theoretical studies of model helicopter rotor broadband noise sources performed at M.I.T. (1-8). Both the low frequency broadband noise (LFBN) and high frequency broadband noise (HFBN) results are presented.

Most work in the past was focused on modeling rotational noise, mainly due to blade slap (9-11). Broadband noise research was mainly overlooked. Major advances were made in this field by our group at M.I.T. and other (12-15). In particular, we have been successful in simulating broadband noise for helicopter rotors, at M.I.T.

Our broadband noise research consisted of both theoretical studies and experimental studies. These studies included two broadband noise sources, namely, i) low frequency broadband noise due to inflow turbulence, and ii) high frequency broadband noise due to boundary layer self noise. Before going into details of present study, a brief discussion of helicopter rotor noise source mechanism is presented in the following paragraph.

1.1 Helicopter Rotor Noise Mechanisms

Depending on their frequency content, the basic source mechanisms of helicopter rotor aerodynamic noise may be classified into two major categories, namely: harmonic/rotational noise, and broadband noise. Refs. (1 to 8). Harmonic noise is identified by discrete narrow peaks which occur at an integer multiple of blade passing frequency. It may be attributed to steady and unsteady blade loading, blade-vortex interaction, thickness effects and shock wave propagation. The latter three are sometimes called blade slap. The harmonic noise spectrum due to steady and unsteady blade loading may extend over 20-25 times the blade passage frequency, whereas in the case of blade slap it may extend over 50-60 times the blade passage frequency. Beyond this range the noise spectrum is continuous and broadband. It is convenient to classify this broadband noise spectrum into two parts: low frequency broadband noise and high frequency broadband noise. The LFBN is mainly attributed to random loading due to inflow turbulence. The HFBN may be due to five mechanisms namely: (a) boundary layer self noise (BLSN), (b) turbulent boundary layer noise, (c) edge noise, (d) incident turbulence noise, and (e) stall noise. BLSN is believed to be a direct consequence of a self excited feedback loop of aerodynamic origin formed by the acoustic wave, laminar boundary layer and angle of incidence. Boundary layer noise is due to boundary layer turbulence. Edge noise is due to the interaction between unsteady flow and the trailing edge. The mechanism of incident turbulence generated noise may extend up to the region where other noise mechanisms discussed under HFBN are operative. Stall noise is due to rapid load fluctuations during stall process or due to the interaction of turbulence in locally stalled region with the rotor blades.

1.2 The LFBN

There are a number of theoretical and experimental studies (3, 5, 6, 12-15) which support turbulence as the source mechanism of LFBN. As the rotor blades pass through a non-uniform velocity field, they experience fluctuating angle of attack causing unsteady lift forces. These random loadings are the result of interaction of the blade with inflow turbulence or with the wake turbulence generated by the same or other blades. As the inflow free stream turbulence contains a spectrum of wave number components, the resulting loading spectrum affects the acoustic spectrum over the entire range of frequencies. A systematic

experimental investigation was carried out to study LFBN from model helicopter rotors at low tip speeds and results are presented. The effects of tip speed, advance ratio, blade loading, size scale and intensity of turbulence on the sound pressure level of LFBN are discussed. A general theoretical model of LFBN is presented. This theory can be used to predict absolute sound pressure levels (SPL) of the LFBN spectrum. In addition, a simplified expression for the peak SPL of LFBN for the case of a sinusoidal gust is developed. This expression is for a single wave number component of a continuous spectrum of a turbulent flow which contains all wave number components. The simple theoretical prediction model for scaling LFBN peak SPL is compared with experimental results.

1.3 The HFBN (due to BLSN)

The discrete tones at high frequencies for stationary airfoils and the high frequency broadband noise hump for rotors operating at subsonic tip Mach numbers may be attributed to laminar boundary layer self noise. This mechanism is highly dependent on Reynolds number and angle of incidence. Experiments indicate that this noise is operative as long as the boundary layer on the airfoil surface or a rotor blade is laminar. It seems that this noise of aerodynamic origin is a direct consequence of a self-excited feedback loop formed by the acoustic wave, laminar boundary layer, and the wake flow of the airfoil. This mechanism is also known as vortex noise because some investigators believe that the noise is due to vortex shedding that is caused by an interaction of the airfoil's wake-induced velocity field and the airfoil itself (16, 17). The shed vortices generate a periodic pressure fluctuation over the airfoil resulting in an edge dipole radiation. This mechanism is also known as discrete tone noise because the spectrum of the noise signal of isolated airfoils within a certain Reynolds number range shows the acoustic power concentrated in a narrow band of frequencies (17). Experimental investigations indicate that these tones are well defined functions of velocity. Since the velocity is continuously varying along the rotor blade span, the tone noise appears as a broadband noise hump for rotors under certain operating conditions.

In this paper, a simple scaling law for HFBN is presented. The experimental investigation of HFBN due to BLSN is based on the same parameters (tip Mach number, advance ratio, etc.) as those for LFBN. This paper also discusses some interesting results of saturation of peak SPL as a function of tip Mach number and advance ratio.

2. Experimental Study

2.1 The M.I.T. anechoic tunnel and rotor facility

The M.I.T. anechoic wind tunnel facility was used for the experimental investigation of broadband noise generated by a model helicopter rotor. The tunnel is an open jet closed circuit wind tunnel designed for low speed aerodynamic experiments. The dimensions of the test section are 1.524 x 2.286 m; top speed is 32.2 m/s. The open jet test section runs through an anechoic chamber of dimensions 7.32 x 3.66 x 3.66 m. The side walls and ceiling of the anechoic chamber is covered with Cremer blocks and the floor of the chamber is covered with 0.152 m. thick polyurethane foam. The anechoic properties of the tunnel were measured and the acoustic cut off frequency above which free field conditions prevail was found to be 160 Hz. The effect of the shear layer of the open jet on refraction and scattering of acoustic waves was studied by using aeolian tones as sound source and was found to be insignificant under the present test conditions. The model helicopter rotor system consists of a 1.27 m diameter rotor. Rotor blades are held by bolts to a root fixture. The rotor hub can take any number of blades up to eight and is connected to a thrust

measuring dynamometer. Details of the rotor and blades are given in Table I.

Controlled turbulence was generated with the aid of biplaner grids mounted in the upstream section of the tunnel. The details of measurement of turbulence properties are described in Ref. 18. Details of turbulence characteristics are given in Table 2 of Ref. 8.

2.2 Instrumentation and data analysis

Figure 1 depicts the schematic of instrumentation for acquisition and reduction of aerodynamic and acoustic data. The details of the instrumentation and data analysis are discussed in Ref. 8.

2.3 Rotor Blade Tip Shapes

Figure 2 shows the geometry of the rotor blades. The interchangeable tips occupy the outer 15 percent of the radius of the rotor blade. The leading edge and the trailing edge sweep angles were selected as 5, 10 and 15 degrees. All blades have the thickness distribution of a NACA 0012 airfoil section. The rotor blades with interchangeable tips consist of a metal spar with balsa wood covered with fiberglass and epoxy. The metal spar extends out from 85 percent radius toward tip. The interchangeable tip shapes slide fit on the metal spar and can be held in position by a metal pin. Details of rotor blade design and fabrication are given in Ref. 19.

2.4 The Test Series

The flowfield associated with a helicopter is quite complex. In order to get a clear understanding of the effect of various parameters of LFBN and BLSN, tests were planned so that only one parameter was varied while keeping the other parameters fixed. The basic parameters were tip speed, advance ratio, blade loading, size scale and intensity of turbulence, and blade tip geometry. In order to form a baseline of the study, square tip blades were tested initially. Then, the results of various tip geometries were compared with the results from the square tip blades. The following paragraph gives the range of various parameters covered in the tests on each geometry.

The tip Mach number was varied from 0.15 to 0.49 which corresponds to the variation in the shaft rpm of 750 to 2500. The advance ratio was varied from 0.075 to 0.25, and the blade loading was varied from 0.057 to 0.12 (obtained from measured thrust). The blade loading covers approximately, the range a typical helicopter encounters. Size scale and intensity of homogeneous turbulence were varied by inserting different grids upstream of the test section of the tunnel. The measured rms intensities of the turbulence were found to be 1.7, 6.25 and 11 percent of the flow velocity at the test section of the wind tunnel for the case of no grid, small grid and large grid, respectively. Whereas, the longitudinal scales of turbulence were found to be 0.2997, 0.0838 and 0.127 meters for the no grid, small grid and large grid, respectively.

For a given state of turbulence in the test section, three sets of tests were planned. For each of the three sets, zero shaft angle was selected. In the first set of tests tip speed was varied by keeping advance ratio and blade loading constant. In the second and third set of tests, advance ratio and blade loading, respectively, were varied keeping other parameters constant. The above set of tests was repeated for square tip blades for the no grid, small grid and large grid cases. Then, each tip geometry was tested in a similar manner. The model rotor consisted of two blades for all tests.

3. Experimental Results

Figure 3 shows a typical spectrum obtained by analyzing a noise signal on the spectrum analyzer. Sound pressure level (SPL) in decibels (dB) is plotted as a function of frequency. The ranges of low frequency broadband noise and HFBN due to boundary layer self noise are shown in this figure. The BLSN range was obtained by putting serrated tape on the rotor blade surface. The serrations were obtained by cutting the tape with pinking shears. The serrated duct tape (.0127 m. wide) was placed at 0.0095 m. from the blade's leading edge. Both suction and pressure side serrations were used. Experiments were conducted to evaluate the effect of either suction side or pressure side serrations. It was found that only the pressure side serrations were effective in reducing the BLSN. The suction side serrations had negligible effect on the BLSN spectrum. This seems to be due to the presence of turbulent boundary layers on the suction surface of the rotor blades.

In our discussion, we refer to a peak SPL as the value of sound pressure level at the intersection of a line which represents the average SPL at lower frequencies of the LFBN spectrum with the SPL axis as shown in Figure 3. The peak SPL of BLSN hump and corresponding peak frequency (frequency at which the peak SPL occurs) are also depicted in this figure.

3.1 LFBN Results

Figure 4 shows the plot of the peak SPL as a function of tip Mach number. For comparison, a line representing sixth power tip Mach number law is also drawn. It is seen that the peak SPL follows approximately a sixth power tip Mach number law. Experiments of (Ref. 18) show that the rms velocity of turbulence, \bar{w} is proportional to the mean flow speed in the test section of the wind tunnel. Since the flow velocity is equal to advance ratio times tip speed, and advance ratio was kept constant at 0.10 during this set of tests, the rms velocity of turbulence is proportional to the tip speed. Therefore, the peak SPL of LFBN follows a tip Mach number to four power law if the effect of rms turbulence velocity is removed by subtracting $20 \log(\bar{w})$ from the peak SPL. This is in accordance with the earlier observation (3) for tip Mach numbers less than 0.20.

It is also seen from Fig. 4 that the SPL curves for the no grid, small grid and large grid cases are successively one above the other. This is due to the increase in rms velocity of turbulence which is highest for the large grid, and lowest for the no grid: and has intermediate value for the small grid.

Figure 5 depicts the effect of advance ratio on the peak SPL of LFBN. It is seen from this figure that the peak SPL of LFBN increases with the advance ratio. This trend is due to the following reasons. First, the advance ratio was increased by increasing the wind tunnel speed. As the rms velocity of inflow turbulence was proportional to the flow/tunnel speed, the peak SPL of LFBN increased with the advance ratio. Second, the advancing rotor blade tip speed was increased by a factor of $(1 + \mu)$. Hence, there was a small increase in the relative velocity of the rotor blade with respect to airflow on the advancing side of rotor by a factor of μ . This contributed to the increases in the SPL of LFBN with increases in advance ratio to a small extent.

A scaling law developed in the following section predicts SPL increase with advance ratio as shown by a line in the figure, for constant tip speed and blade loading. The prediction appears to be in a good agreement with the experimental data. Again, the SPL curves for the no grid case, the small grid case and the large grid case are successively one above the other. This is again due to the monotonic increase in the rms velocity of the inflow turbulence which is highest for the large grid and lowest for the no grid case.

Figure 6 shows the peak SPL variation with the blade loading for no grid, the small grid and the large grid cases. This figure shows that the peak SPL of LFBN increases with the blade loading and is a function of the rms intensity of turbulence. It also shows that for a given grid (rms intensity of turbulence), the peak SPL of LFBN increases with blade loading.

It may be noted that the theories (12-15) do not predict any increase in the sound pressure level with increases in blade loading keeping all other parameters fixed. The present experimental study has revealed that the SPL is a function of the blade loading. This is important because the helicopter rotors do not operate at constant blade loading. Even for a given blade loading, the SPL predicted by the LFBN theories may be different from the experimental results. This is because the theories developed earlier do not incorporate the mechanism of noise generation as a function of blade loading.

To further understand the increase in the peak SPL with blade loading, we conducted two additional sets of experiments. These experiments were conducted to find out whether the tip path plane (and therefore, the rotor wake) and inflow velocity had any effect on the observed increases. Effects of tripping the boundary layer by using serrations and forward tilting of rotor shaft were studied. The test results were similar to those obtained earlier. Thus, it is still not clear why the SPL of LFBN should increase with blade loading and should depend on the intensity of rms turbulence.

Figure 7 shows a typical comparison for the TE geometry with the square tip. This figure corresponds to tests at constant blade loading of 0.106, keeping tip speed and tunnel speed constant and for the no grid case. It is seen that the SPL reductions of the order of 2-5 db can be obtained at the lower end of the LFBN spectrum. The SPL reductions were found to be higher for larger sweep geometries. However, for the blades with larger sweep angles, the thrust levels at high blade loadings were found to be smaller compared to those for the square tip blades. From the point of view of the thrust levels at high blade loadings, our results indicated that the sweep angles should be limited to about ten degrees.

Tests were also conducted for the small grid and large grid cases. Somewhat smaller SPL reductions were observed for various tip geometries compared to those for no grid case. The reductions observed were found to be closely related to SPL variations.

3.2 BLSN Results

The peak SPLs of BLSN hump are plotted as a function of tip Mach number in Figure 8. The effect of different grids on the peak SPL of BLSN is also included in this figure. For a given grid case, it is observed that the peak SPL of BLSN appears to saturate or fall off as the tip Mach number is increased. This observed trend is different from that reported earlier in Ref. 20. It was reported in Reference 20 that the peak SPL followed a 5.8 power law of advancing blade tip Mach number for tip Mach numbers less than 0.20 in the no grid case.

The explanation of this can be given based on the characteristics of the BLSN phenomena. It should be noted that this phenomena is highly dependent on the Reynolds number and the angle of attack. In fact, serration studies indicated that a considerable reduction in the SPL of the BLSN peak was observed with the proper use of serrations (Ref. 2, 20). The effect of serrations on blade surface is to change the boundary layer from a laminar to a turbulent one. Also, it was observed by Paterson, et. al. (Ref. 21) that the sound pressure level associated with discrete tones on stationary airfoils was a strong function of the Reynolds number and the angle of attack (which, in turn, are related to type of boundary layer on airfoil surface). Paterson, et. al. (Ref. 21) also

observed that the far field tone amplitudes increased rapidly with velocity for low velocities or Reynolds numbers, then the amplitudes saturated and fell off rapidly after saturation for the airfoil at a given angle of attack. Our experiments on model helicopter rotors also show similar dependence on the velocity and angle of attack. It seems that up to a Mach number of 0.20, the peak SPL of BLSN peak increases as $M^{5.8}$ law as reported earlier by Refs. 1, 2, 20 and then saturation or reduction in the peak SPL occurred when the tip Mach number was varied from 0.20 to 0.40.

Note from Figure 8 that the peak SPL associated with the test results for small and large grid are lower than those for no grid case. This seems to be due to the influence of inflow turbulence on laminar boundary layers on the rotor blade surfaces. The observation of reduction in the peak SPL of BLSN with increase in inflow turbulence intensity was also reported earlier. (Ref. 2)

Figure 9 shows the effect of tip Mach number on the peak frequency of BLSN hump for no grid case. As discussed earlier, the peak frequency increases with tip Mach number. The slope of frequency (Hz) versus tip velocity (ft/s) was found to be 28, as compared to 54 reported in Reference 2. The explanation for this may be given in the following way.

As the tip velocity is increased beyond Mach number 0.20 it is believed that contribution to SPL from outermost region does not increase with $M^{5.8}$ law and some portion of tip region of rotor blade radiates equal amplitude of sound due to saturation phenomena. The area of this outer tip region radiating saturated amplitude of sound gradually increases with tip speed. Therefore, the peak frequency cannot be assumed to scale with the Strouhal number based on tip velocity because a portion of the outer blade tip region radiates saturated amplitude of sound. In fact, the Strouhal scaling law now should use a velocity less than the tip velocity. If the Strouhal number is still assumed to be based on the tip velocity, then naturally the slope of $f - V_t$ plot would decrease. It may be noted that the saturation in amplitude for stationary airfoils is dependent on both the Reynolds number and the angle of attack and care should be taken in applying this result for helicopter rotors since for rotors in simulated forward flight, the Reynolds number and angle of attack of a rotor blade element depends on the radial and azimuthal locations.

Figure 10 depicts the effect of advance ratio on the peak SPL of BLSN for a two-bladed rotor. The results again show either saturation or fall-off in the peak SPL of BLSN with increases in advance ratio. This may be compared to previously observed 8 dB per doubling of advance ratio (Ref. 2). The explanation for the observed trends of the effects of advance ratio in the present study are closely related to those discussed earlier for the effects of tip Mach number.

To determine the effect of blade loading on the spectrum and intensity of BLSN, the pitch setting of rotor blades varied while maintaining the rotor rotational speed at 1500 rpm and advance ratio at 0.10. Figure 11 shows the spectrum shapes for no grid case. It is seen from this figure that the peak SPL increases with increases in blade loading. This increase seems to be due to increases in the angle of attack. The increase in angle of attack allows a more favorable pressure gradient on the pressure side of the rotor blade surface. The favorable pressure gradient in turn delays the transition of laminar boundary layer.

Experiments were conducted on three leading edge and three trailing edge swept rotor blade tip geometry are shown in Figure 12. Effect of both side serrations is also included. It is seen that the serrations have a pronounced effect on the reduction BLSN than the 15 degree trailing edge sweep. Results of leading edge sweep blade tips are discussed in detail in Refs. 7 and 19.

Experiments were conducted on three leading edge and three trailing edge swept rotor blade tip geometries. Typical results for trailing edge geometry are shown in Figure 12. Effect of both side serrations is also included. It is seen that the serrations have a pronounced effect on the reduction BLSN than the 15 degree trailing edge sweep. Results of leading edge blade tips are discussed in detail in Refs. 7 and 19.

4. Theoretical Study

In this section, theoretical models of both LFBN and HFBN are discussed. In particular, a general theory of LFBN is presented and scaling laws for both LFBN and HFBN are given.

4.1 Theory for LFBN

4.1.1 General Theory

Brief details of a general theoretical model⁶ are discussed here. This theory predicts absolute sound pressure levels of the low frequency broadband noise due to inflow turbulence. This requires details of inflow turbulence characteristics in predicting the acoustic spectrum.

The following are the important features which will be used in the present formulation. The high frequency assumption¹² is used in the analysis. This approximation allows the sound pressure to be calculated as if the rotor blades were instantaneously in rectilinear motion. The sound generated by an airfoil in rectilinear motion in terms of present coordinates (rather than retarded coordinates) is given in Ref. 22. This gives the acoustic spectrum produced by an airfoil encountering turbulence as measured by an observer fixed with respect to the airfoil. To determine the spectrum in a ground fixed system a Doppler shift is applied.

The procedure of theoretical analysis is similar to that given in Refs. 12, 13, 22. However, the following modifications are made. The effect of blade twist and blade flapping is incorporated to accurately define the noise directivity pattern of each blade segment. A detailed expression for the chordwise integral of the airfoil response function is given. Based on the experimental results, the effect of blade to blade correlations is not included, i.e., correlation of sound from one blade passage with the sound from a different blade passage is ignored. This assumption should be valid for helicopter rotors but may not be appropriate for compressors and turbines with many blades.

The final expression for the averaged power spectral density (PSD) of acoustic pressure is given by (see for details Ref. 6 and 19).

$$S_{pp}(x, y, z, \omega) = \iint_{00}^{2\pi R} dr d\psi \left(\frac{\omega}{\omega_0}\right)^2 \left\{ \frac{\omega z \rho_0 c |L|}{4c_0 \sigma_1^2} \right\}^2 \phi_{ww}(K_x, \frac{\omega Y}{c_0 \sigma_1}) \cdot V \quad (1)$$

where

$$L(x, K_x, k_y) = \int_{-1}^1 d\xi g(\xi, K_x, k_y) e^{-\frac{i\omega\xi c}{2c_0\beta^2} (-M + \frac{x}{\sigma_1})} \quad (2)$$

$$\phi_{ww}(k_x, k_y) = \int_{-\infty}^{\infty} dk_z \phi_{ww}(k_x, k_y, k_z) \quad (3)$$

$$K_x = -\frac{\omega}{V} \quad (4)$$

and

$$\sigma_1 = \sqrt{x^2 + \beta^2(y^2 + z^2)} \quad (5)$$

The quantities x, y, z , in right side of Eq. (1) are the relative coordinates of the observer with respect to the present location of the airfoil. The square of Doppler factor was introduced in Eq. (1). One factor is introduced to keep constant the energy in a given percent bandwidth when frequency is Doppler shifted. The other factor is introduced to account for the fact that the rotor spends different amounts of retarded time at different azimuthal locations (see Ref. 12). Once the function L and the turbulence field is known then the PSD of acoustic pressure can be calculated from Eq. (1).

Numerical calculations were made to predict the sound pressure levels of LFBN from model helicopter rotor in forward flight. Equation (2) was used in the numerical computations. Figure 13 shows a typical comparison of theoretical and experimental results for the case of the effect of advance ratio on LFBN, with turbulence generated by the small grid. The theoretical results are in good agreement with the experimental results. Since the HFBN is operative at low rotor rpm and at high frequencies, theory does not agree with the experiment at the high frequency end of the LFBN spectrum. However, if the serrations had been used in the experiments, then the agreement would have been better over almost the entire frequency range shown in these figures. Note that the HFBN hump occurs at high frequencies for a rotor rpm of 2000, hence, the theoretical results agree with the experimental results up to about 8000 Hz. Details of the complete comparisons are discussed in Ref. 6 and 19.

4.1.2 Scaling Formula

Several expressions (6, 12-15) for the prediction of LFBN are quite involved and it becomes difficult to obtain a simplified picture of how the peak sound pressure level varies with different rotor parameters. The fact that the LFBN falls off rapidly with frequency can be used to simplify the expressions for the peak SPL predictions, since the peak SPL occurs at the low frequency end of the LFBN noise spectrum.

We start with Lowson's expression²³ for the sound field of a point dipole in an arbitrary motion. For a rotor blade at advancing position, where maximum sound power is emitted by blades, and encountering a sinusoidal convected gust, we can write a simple relation for $|p|^2$ as follows.

$$|p|^2 \approx \left(\frac{\cos\theta p_0 \bar{w}}{c_0 r_1} \right) \frac{cR}{50} V_t^4 (1 + 5\mu + 10\mu^2) \left(\frac{f}{\Omega} \right). \quad (6)$$

This expression states that for the sinusoidal gust the SPL is proportional to the square of rms velocity of gust and to the fourth power velocity law. The above formula, although not exact, gives an idea of how the sound pressure level would vary as a function of rotor parameters. The above expression may be used to scale the peak SPL of a helicopter rotor due to turbulent inflow. The assumptions in deriving it are:

- (i) acoustic far-field is assumed,
 $R/r_1 \ll 1$
- (ii) $\omega \gg \Omega$
- (iii) $\beta^2 \approx 1$,
- (iv) $\left(\frac{c}{\lambda \beta^2} \right)^2 \ll 1$,
- (v) $M\pi \left(\frac{c}{\lambda \beta^2} \right) < 1$,
- (vi) $\frac{2\pi^2}{M} \left(\frac{c}{\lambda^3} \right) > 1$, (7)

The trends of the peak SPL of LFBN with tip speed and advance ratio keeping other parameters fixed is found to be in a good agreement with the experimental results. Figures 4 and 5 show such comparisons for the effect of tip speed and advance ratio, respectively. The trends of the peak SPL variation with tip speed and advance ratio for no grid, small grid and large grid case are well predicted by the scaling law. It may be noted that the present theory does not include the effect of blade loading on the SPL of LFBN.

4.2 Theory for HFBN (BLSN)

In this section, we discuss theoretical model for BLSN. Note that, in Refs. 1, 18, the BLSN is referred to as HFBN.

To obtain a similar scaling procedure for high frequency broadband noise due to BLSN generated by a model rotor, we assumed that noise sources were acoustically compact and computed the instantaneous pressure due to an element of an airfoil where vortices are being shed. Extending experimentally obtained results for the spanwise correlation lengths for stationary airfoils to rotating airfoils and assuming that the correlation lengths vary like the displacement thickness of the boundary layer, it was observed that the peak intensity of high frequency broadband noise BLSN has a $V_t^{5.8}$ factor. An expression which scales the location of peak intensity in the frequency domain was obtained based on the rotor blade geometric parameters. The resulting scaling laws for peak intensity^{1, 18} was found to be

$$\begin{aligned} \text{SPL}_2 = \text{SPL}_1 + 60 \log \frac{M_{t_2}}{M_{t_1}} + 20 \log \frac{c_2 t_1}{c_1 t_2} \\ + 10 \log \frac{B_2}{B_1} - 20 \log \frac{r_2}{r_1} + 10 \log \frac{(\Delta L)_2}{(\Delta L)_1} \\ + 10 \log \left\{ \left(1 + \frac{14}{3} \mu_2 + \frac{42}{5} \mu_2^2 \right) \right. \\ \left. / \left(1 + \frac{14}{3} \mu_1 + \frac{42}{5} \mu_1^2 \right) \right\} \quad (8) \end{aligned}$$

and the peak frequency was found to be given by

$$f_{p_{1,2}} = 1.08 V_{t_{1,2}} / t_{1,2} \quad (9)$$

for two rotor systems (designated by suffixes 1 and 2).

The effects of intensity and size scale of turbulence were less obvious in the study of high frequency broadband noise (BLSN). One of the effects of free stream turbulence is to alter the correlation lengths of shed vortices (24). To this end, we used an existing integral boundary layer calculation to predict the turbulent boundary layers developing in a turbulent free stream. The results indicated that increase in the intensity of free stream turbulence in general, would tend to decrease the correlation length, thus resulting in reducing the intensity of BLSN.

A comparison of predicted peak frequency and sound pressure levels with experimental data showed good agreement except for the case of effect of turbulence on the intensity of BLSN for tip Mach numbers less than 0.20. However, above tip Mach number 0.20, we observed saturation in the peak SPLs of BLSN

(as discussed in section 3.2). Thus, the present scaling law is valid up to a tip Mach number of 0.20 for M.I.T. model helicopter rotor.

5. Conclusions:

Results of experimental and theoretical investigation of broadband noise radiated from model helicopter rotors are presented. Conclusions are summarized for both the LFBN and HFBN (due to BLSN) below.

5.1 LFBN

1) The experimental results on the effect of tip speed and advance ratio on the peak SPL of LFBN can be explained on the basis of present LFBN theories.

2) The experimental results on the effect of blade loading on the peak SPL of LFBN is still not clearly understood.

3) The experimental results showed 2-5 dB reductions for swept geometries compared to square tip blades at constant blade loading.

4) A general theoretical model is discussed which can be used to predict absolute sound pressure levels of LFBN due to inflow turbulence. Theoretical results were found to be in good agreement with the experimental results.

5) A simple peak SPL scaling law for noise from helicopter rotor in forward flights due to a convected sinusoidal gust is developed. The trends of variation of peak SPL of LFBN with advance ratio and tip speed predicted by the scaling law showed very good agreement with the experimental results.

5.2 HFBN due to BLSN

1) The peak SPL of BLSN showed either saturation or fall-off as the tip Mach number was increased from 0.20 to 0.40 and advance ratio was increased from 0.075 to 0.250.

2) The magnitude of peak SPL of BLSN hump decreased with an increase in inflow turbulence intensity.

3) The peak frequency of BLSN hump increased somewhat slowly with rotor blade tip velocity, as compared to that observed earlier and reported in Ref. 2.

4) The magnitude of peak SPL of BLSN was found to increase with blade loading.

5) The BLSN hump seems to become broader with increases in blade sweep angle. The peak SPL of BLSN was found to decrease with an increase in the trailing edge sweep angle.

6) Serrations on both rotor blade surfaces had pronounced effect on the reduction of BLSN. Suction side serrations had negligible effect on the reduction of BLSN, as compared to pressure side serrations.

7) The mechanism of BLSN seems to be closely related to the presence of laminar boundary layers on rotor blade surfaces. The BLSN is found to be sensitive to both Reynolds number and blade loading.

8) The scaling law for BLSN is found to predict the experimental results upto tip Mach number of 0.20. Experimental results indicate that saturation effects are important above tip Mach number of 0.20.

Acknowledgements:

This research program was partially supported by the U. S. Army Research Office (Contact no. Daag 2g-C-027), and by the NASA (Grant Nos. NSG-2095 and NSG - 1583).

References:

1. Aravamudan, K., Lee, A., and Harris, W. L., "A Simplified Mach Number Scaling Law for Helicopter Rotor Noise," J. of Sound and Vibration, Vol. 57, No. 4, 1978.
2. Aravamuden, K., Lee, A., and Harris, W. L., "An Experimental Study of High Frequency Noise from Model Rotors: Prediction and Reduction," Vertica, Vol. 3, 1979.
3. Aravamudan, K. S., and Harris, W. L., "Low Frequency Broadband Noise Generated by a Model Rotor," J. Acoust. Soc. Am., Vol. 66, No. 2, August 1979.
4. Humbad, N. G. and Harris, W. L., "On the Acoustic Power Emitted by Helicopter Rotor Blades at Low Tip Speeds," J. of Sound and Vibration, Vol. 66, 1979.
5. Humbad, N. G., and Harris, W. L., "Model Rotor Low Frequency Broadband Noise at Moderate Tip Speeds" AIAA 6th Aeroacoustics Conference, June 4-6, 1980, Hartford, Conn., AIAA Paper 80-1013.
6. Humbad, N. G., and Harris, W. L., "Tip Geometry Effects on the Model Helicopter Rotor Low Frequency Broadband Noise" AIAA 7th Aeroacoustics Conf., Oct. 5-7, 1981, Palo Alto, California, AIAA Paper 81-2003.
7. Humbad, N. G., and Harris, W. L., "On High Frequency Broadband Noise from Model Helicopter Rotors", AIAA 8th Aeroacoustics Conf., April 11-13, 1983, Atlanta, Georgia, AIAA Paper 83-0673.
8. Humbad, N. G., and Harris, W. L., "Model Helicopter Rotor Low Frequency Broadband Noise", Vertica, Vol. 6, 1982.
9. Lee, A., Harris, W. L., and Widnall, A., "An Experimental Study of Helicopter Rotor Rotational Noise in a Wind Tunnel," Journal of the Aircraft, Vol. 14, No. 11, 1977.
10. Yu, Y. H., Caradonna, F. X., and Schmitz, F. H., "The Influence of the Transonic Flow Field on High-Speed Helicopter Impulsive Noise," 4th European Rotorcraft and Powered Lift Aircraft Forum, Paper No. 58, Stresa, Italy, September 13-15, 1978.
11. Leighton, K. and Harris, W. L., "A Parametric Study of Blade/Vortex Interaction Noise for Two, Three and Four Bladed Rotors at Moderate Tip Speeds: Theory and Experiment." 39th Annual AHS Forum and Technology Display, Paper No. A-83-39-52-D000, St. Louis, MO, May 9-11, 1983.
12. Paterson, R. W., and Amiet, R. K., "Noise of a Model Helicopter Rotor due to Ingestion of Turbulence," NASA-CR, No. 3213, 1979.
13. Amiet, R. K., "Noise Produced by Turbulent Flow into a Propeller or Helicopter Rotor," AIAA Paper No. 76-560, 1976.

14. George, A. R. and Chou, S. T., "Comparison of Broadband Noise Mechanisms, Analyses, and Experiments on Helicopters, Propellers, and Wind Turbines," AIAA Paper 83-0690, 1983.
15. George, A. R., and Kim, Y. N., "High Frequency Broadband Rotor Noise," AIAA J., Vol. 15, No. 4, pp. 538-545, April 1977.
16. Tam, C. K. W., "Discrete Tones from Isolated Airfoils," J. of Acoust. Soc. Am., Vol. 55, 1974, pp. 1173-1177.
17. Hersh, A. S., Soderman, P. T., and Hayden, R. E., "Investigation of Acoustic Effects of Leading Edge Serrations on Airfoils," J. of Aircraft, Vol. 11, No. 4, 1974, pp. 197-202.
18. Aravamudan, K., "Effects of Free Stream Turbulence on Model Helicopter Rotor Noise," D. Sc. Thesis, M. I. T., Cambridge, MA, September 1977.
19. Humbad, N. G., "Effect of Tip Geometry and Performance Parameters on Model Helicopter Rotor Broadband Noise," Ph. D. Thesis, M. I. T., Cambridge, MA, 1981.
20. Lee, A., Aravamudan, K., Bauer, P., and Harris, W. L., "An Experimental Investigation of Helicopter Rotor High Frequency Broadband Noise," AIAA Paper 77-1339, 1977.
21. Paterson, R. W., Vogt, P. G., Fink, M. R., "Vortex Noise of Isolated Airfoils," J. of Aircraft, Vol. 10, No. 5, May 1973, pp. 296-302.
22. Amiet, R. K., "Acoustic Radiation from an Airfoil in a Turbulent Stream," J. of Sound and Vibration, Vol. 41, No. 4, 1975, pp. 407-420.
23. Lowson, M. V., "The Sound Field for Singularities in Motion," Proc. Royal Soc., A2869, pp. 559-572, 1965.
24. Schlinker, R. H. and Brooks, T. F., "Progress in Rotor Broadband Noise Research," 38th Annual AHS Forum and Technology Display, Anaheim, CA, May 4-7, 1982.

Table 1. Model rotor characteristics

Radius (R)	0.635 m
Chord (c)	0.0508 m
Number of blades (B)	1 to 8
Section	NACA 0012
Twist	-8 degrees
Shaft tilt capability	± 20 degrees
Testing rpm range	400 to 2650
Lead-lag	None
Cyclic pitch	None
Collective pitch	By adjusting pitch of individual blade

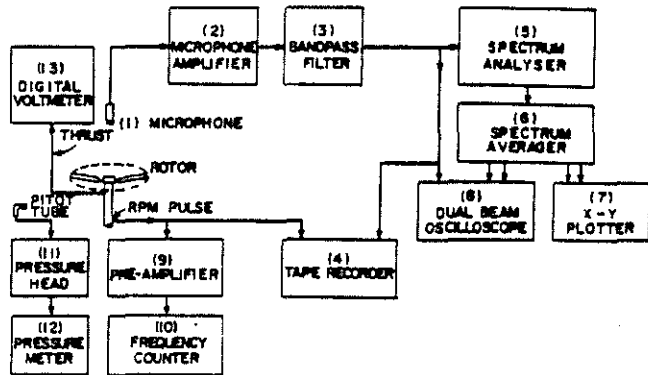


Fig. 1. Schematic of instrumentation for broadband noise study.

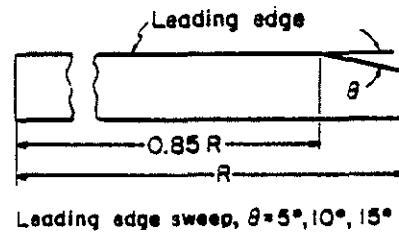
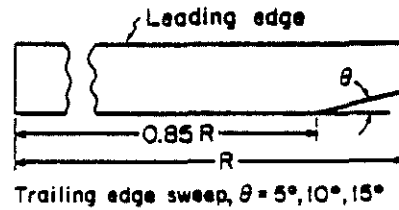


Fig. 2 Rotor blade tip shapes.

Table 1. Model rotor characteristics

Radius (R)	0.635 m
Chord (c)	0.0508 m
Number of blades (B)	1 to 8
Section	NACA 0012
Twist	- 8 degrees
Shaft tilt capability	\pm 20 degrees
Testing rpm range	400 to 2650
Lead-lag	None
Cyclic pitch	None
Collective pitch	By adjusting pitch of individual blade

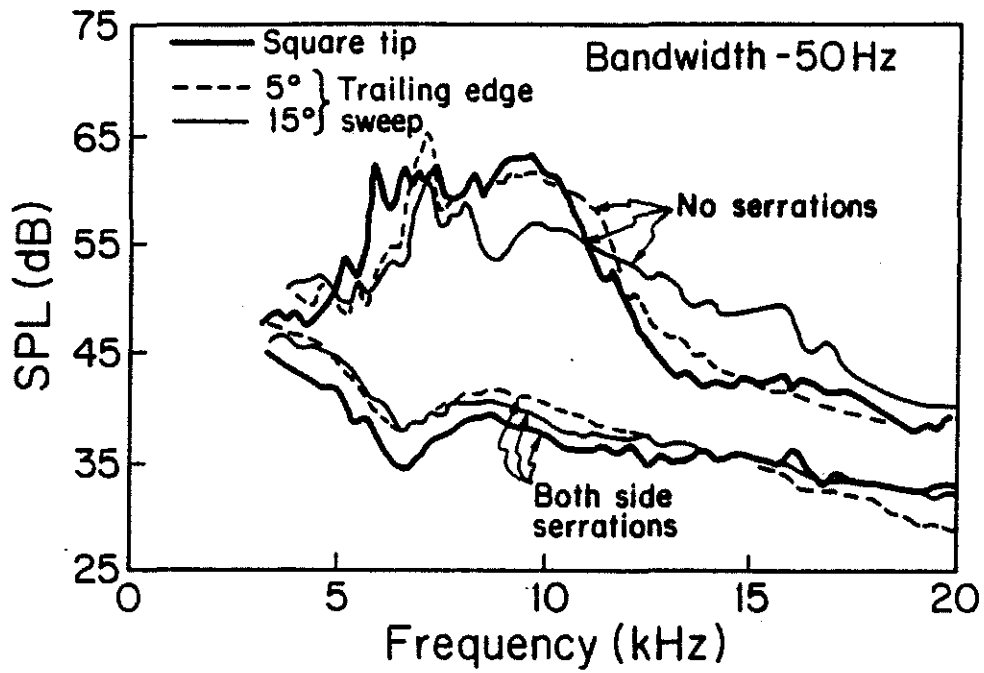


Fig. 3 Ranges of LFBN and HFBN (BLSN), no grid, 1500 RPM.

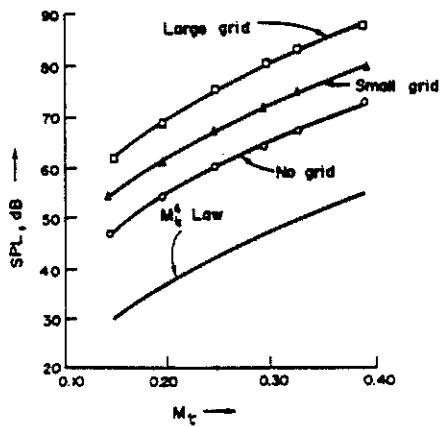


Fig. 4 Effect of rotational Mach number on peak SPL of LFBN (effect of RMS turbulence velocity is not removed).

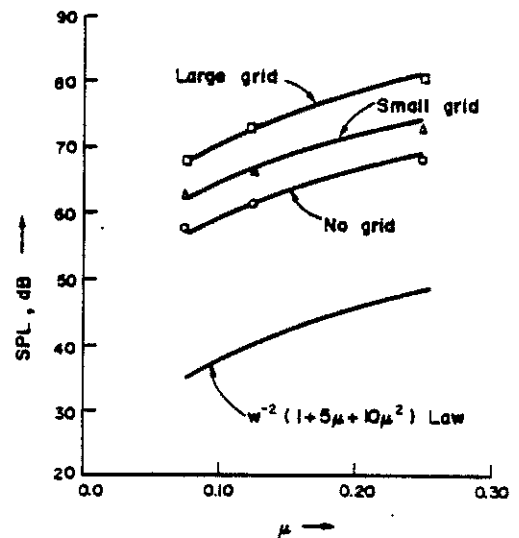


Fig. 5 Effect of advance ratio on the peak SPL of LFBN.

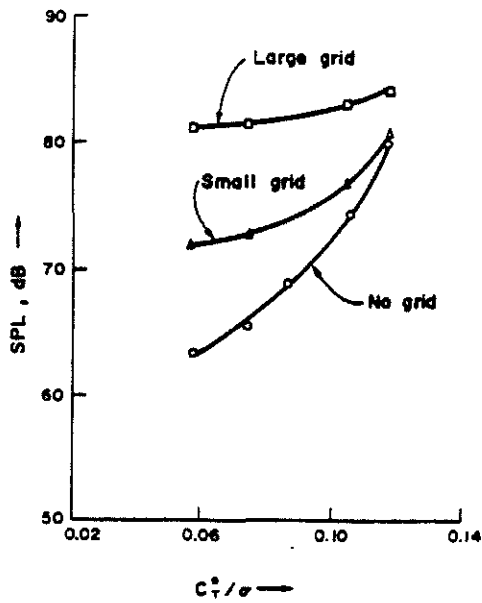


Fig. 6 Effect of blade loading on peak SPL of LFBN.

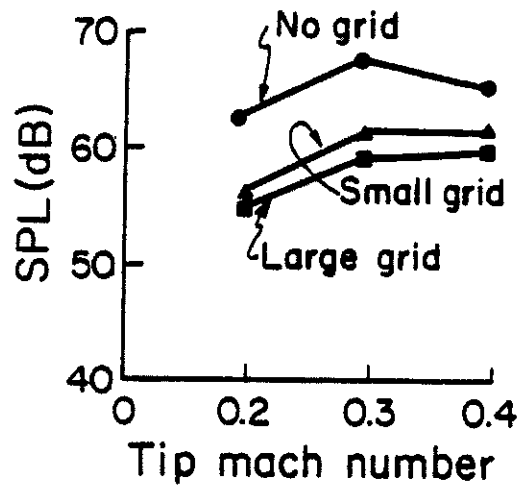


Fig. 8 Effect of tip Mach number on the peak SPL of LFBN.

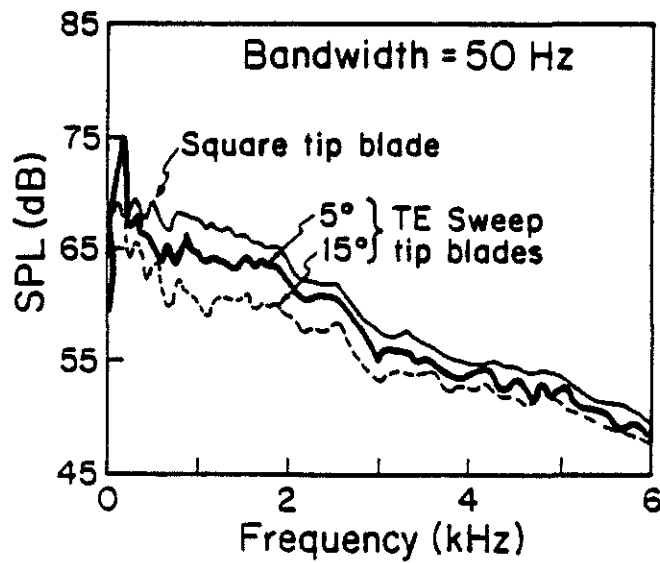


Fig. 7. Effect of TE sweep tip shapes on the SPL of LFBN at constant blade loading, No Grid for $B=2$, $V_t=99.8$ m/s, and $\mu=0.10$.

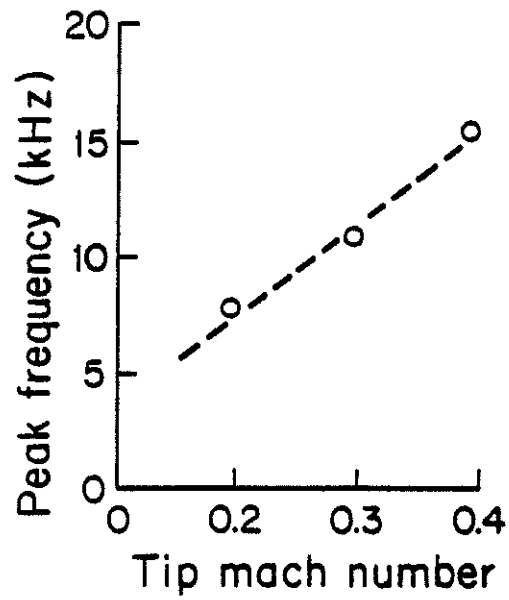


Fig. 9 Effect of tip Mach number on the peak frequency of BLSN hump.

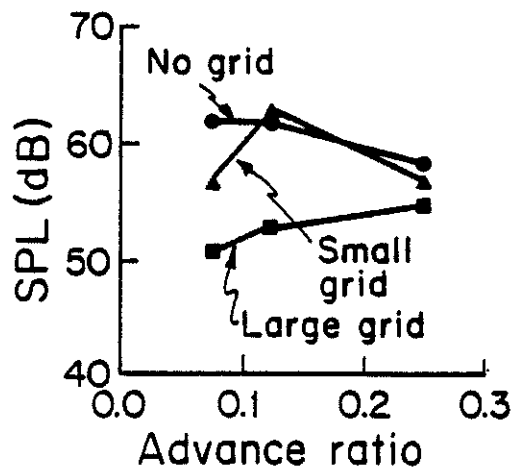


Fig. 10 Effect of advance ratio on peak SPL of BLSN.

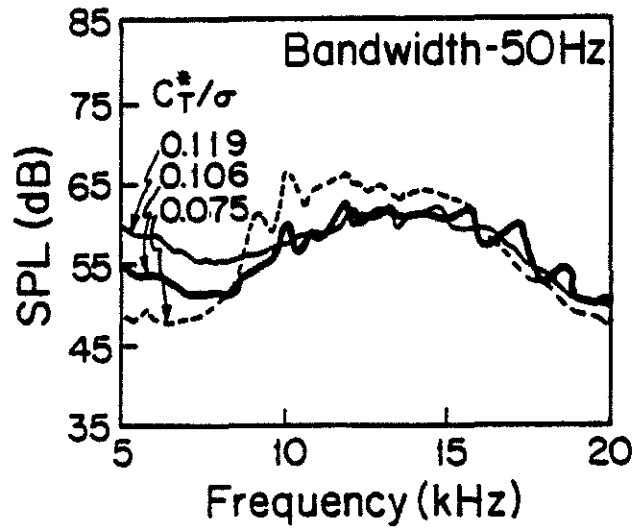


Fig. 11. Effect of C_T^*/σ , no grid, square tip.
 C_T^* - measured blade loading
 σ - solidity ratio

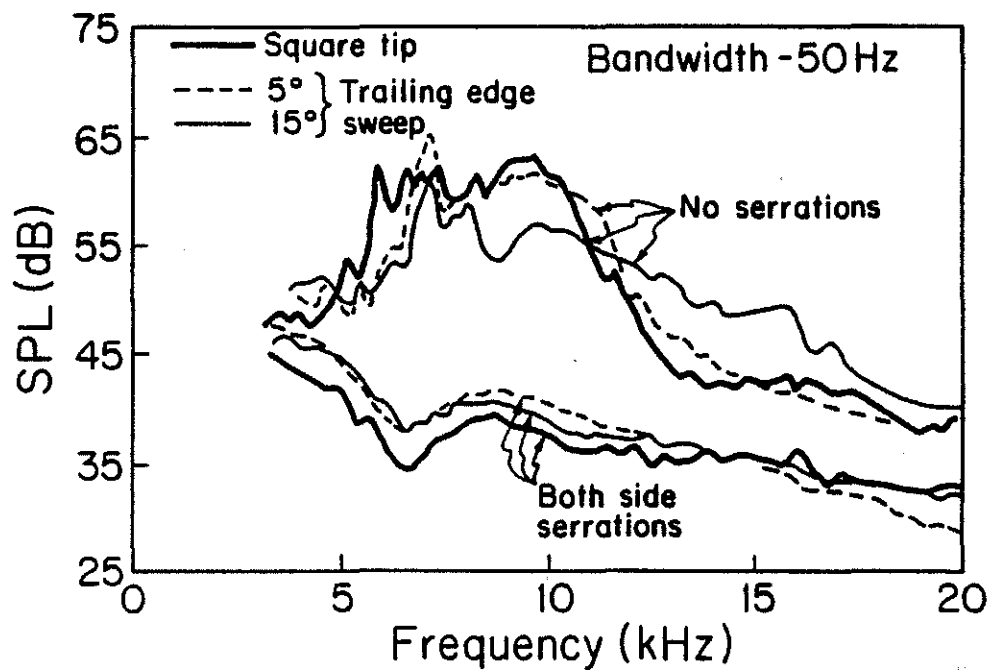


Fig. 12. Effect of serrations and sweep on BLSN, no grid.